

# A nonlinear empirical I/V model for GaAs and GaN FETs suitable to design power amplifiers

Daniel Ochoa-Armas<sup>1</sup>  | Ismary Lavandera-Hernández<sup>1</sup>  |  
 Daniel Fernández-Ramón<sup>1</sup> | José R. Loo-Yau<sup>1</sup>  | Marlon Molina-Ceseña<sup>2</sup> |  
 Caín Pérez-Wences<sup>3</sup>  | Ernesto A. Hernández-Domínguez<sup>1</sup> |  
 J. Apolinar Reynoso-Hernández<sup>2</sup>  | Pablo Moreno<sup>1</sup>

<sup>1</sup>Centro de Investigación y Estudios Avanzados del I. P. N. Unidad Guadalajara, Zapopan, Jalisco, Mexico

<sup>2</sup>Centro de Investigación Científica y Estudios Superiores de Ensenada, Ensenada, Baja California, Mexico

<sup>3</sup>Department of Electronics and Control, Centro de Tecnología Avanzada CIATEQ A. C., Zapopan, Jalisco, Mexico

## Correspondence

Daniel Ochoa-Armas, Centro de Investigación y Estudios Avanzados del I. P. N. Unidad Guadalajara, Av. Científica 1145, Colonia El Bajío, C. P. 45015, Zapopan, Jalisco, Mexico.  
 Email: daniel.ochoa@cinvestav.mx

## Funding information

Consejo Nacional de Ciencia y Tecnología, Grant/Award Numbers: 163272, 206029

## Abstract

This article presents an improved nonlinear empirical I/V model suitable for GaAs and GaN FETs. The new drain-to-source current formulation accurately represents the symmetric and the asymmetric bell-shaped transconductance ( $g_m$ ) for all  $V_{DS}$  values. Besides modeling with high accuracy the I/V characteristic, the proposed model can fit the first and second derivatives of the transconductance, from the ohmic to the saturation region, including the pinch-off region. The high correlation between experimental and simulated data of the I/V curves of GaAs and GaN FETs, ACPR, load-pull, and a class-J power amplifier designed in S-band corroborates the usefulness of the proposed model, considering only the static I/V model as the main nonlinear element of the electrical equivalent circuit model of the transistor.

## KEY WORDS

empirical I/V model, MET model, microwave FET model, nonlinear model

## 1 | INTRODUCTION

In the design of microwave circuits based on field-effect transistors (FETs), accurate nonlinear models are required. The nonlinear FET model consists of static or pulsed I/V characteristics and the Q/V charge based model. I/V models are used to predict not only the bias dependent current source ( $I_{DS}$  [ $V_{GS}, V_{DS}$ ]), but also its derivatives: output conductance ( $g_{ds}$ ) and transconductance ( $g_m$ ). Besides, the high-order derivatives of  $g_m$  are related to the harmonics and intermodulation analysis.

In the nonlinear modeling of FETs using electrical equivalent circuits (EECs),  $I_{DS}$  ( $V_{GS}$ ,  $V_{DS}$ ) is the main nonlinear distortion generator.<sup>1</sup> Hence, it is the most crucial nonlinear element to model. The  $I_{DS}$  ( $V_{GS}$ ,  $V_{DS}$ )

nonlinearity is mostly related to strong nonlinearities in the ohmic to saturation transition, pinch-off, and forward regions, besides the intrinsic nonlinearities like the output conductance and transconductance bias dependence.<sup>1,2</sup>

The basis for modeling the nonlinear current source  $I_{DS}$  ( $V_{GS}$ ,  $V_{DS}$ ) is through a static model.<sup>1</sup> Then thermal and trapping effects are modeled introducing the temperature dependence in the static model, using sub-circuits that model the traps' capture and emission time. Finally, the capacitance/charge model is used to consider the dynamic behavior of the FET. Nevertheless, a complete nonlinear FET model with all the features mentioned above is less accurate if there is not present an accurate  $I_{DS}$  ( $V_{GS}$ ,  $V_{DS}$ ) nonlinear model.

Several semi-empirical analytical  $I_{DS}$  ( $V_{GS}$ ,  $V_{DS}$ ) modeling techniques for GaN and GaAs HEMT devices have

been developed,<sup>3–18</sup> for example, table-based Artificial Neural Networks (ANNs), or analytical modeling techniques. The table-based model represents each element to be modeled with a lookup table developed from measured data. Although it is easy to implement, this modeling technique cannot predict out-of-range measurements and has convergence problems when dealing with nonlinearities. The ANN modeling technique has higher accuracy even under strong nonlinear operating conditions; however, it has limited prediction capability. The analytical modeling is more efficient in terms of convergence and prediction capability; however, it requires an effort to improve its performance in all regions of the I/V curves.

In that sense, several empirical I/V models for microwave FETs, based on analytical expressions, have been developed. Two of the most accepted analytic formulations are the Angelov-Zirath model<sup>3</sup> and the industry-standard MET<sup>19</sup> model. Both models were modified to make them more suitable for describing transconductance behavior and its dependence on  $V_{DS}$ . In the case of the model from Reference 3, one of its characteristics is the accurate modeling of the peak of the transconductance<sup>4,11,15,16,20</sup> in MESFET and GaN devices. On the other hand, the most notable modification of Reference 19 is the work from Fager<sup>21</sup> to model the  $I_{DS}$  characteristic of LDMOS devices.

With fewer fitting parameters than the other mentioned models, Reference 21 has successfully modeled the  $I_{DS}$  ( $V_{GS}$ ,  $V_{DS}$ ) characteristic of GaN transistors,<sup>5–8,10</sup> achieving good performance in representing the transconductance when biasing the transistor in the saturation region. Particularly for GaN devices, all the models mentioned above have a common factor: they are suitable for modeling the highly asymmetric bell-shaped transconductance that appears when the FET is in the saturation region ( $V_{DS} > V_{knee}$ ). However, none of them deals with the quasi-symmetrical bell-shaped form, which is present when the device is biased with a  $V_{DS}$  in the ohmic region.<sup>22</sup> As an example of this, Figure 1 shows a comparison of measured and simulated  $I_{DS}$  –  $V_{GS}$  data for a HEMT GaN CGH40045F, where the simulation, based on the I/V model of Reference 21, shows a low correlation with measured data in the ohmic region, being this more evident for values of  $V_{GS}$  close to the threshold voltage.

In this article, using the  $I_{DS}$  ( $V_{GS}$ ,  $V_{DS}$ ) formulation from Reference 21, we develop an improved nonlinear empirical I/V model capable of modeling the transconductance characteristic and its dependence with  $V_{DS}$  of HEMT GaAs and high power GaN devices. To achieve the above, we have included two functions from Reference 4 and introduced a new function that helps to model the transconductance accurately for low and high values of  $V_{DS}$ . Using pulsed I/V measurements of a packaged

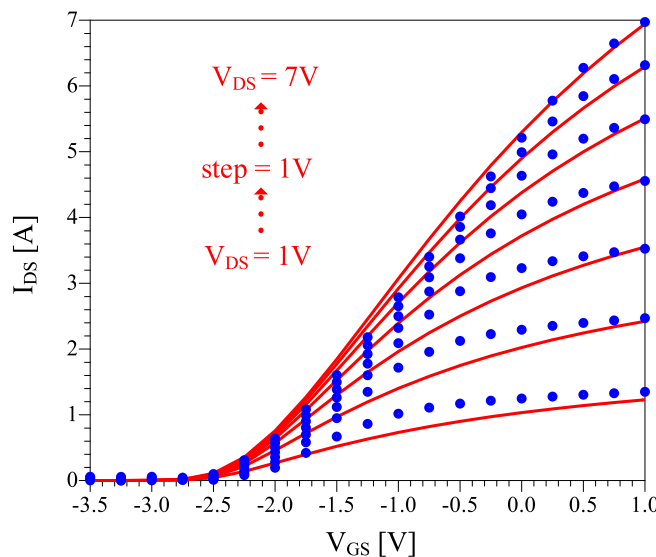


**FIGURE 1** Comparison of measured (circle) and simulated data using the model from Reference 21 (solid line), for a packaged GaN HEMT CGH40045F at a  $V_{GSq} = -2.5$  V and  $V_{DSq} = 28$  V

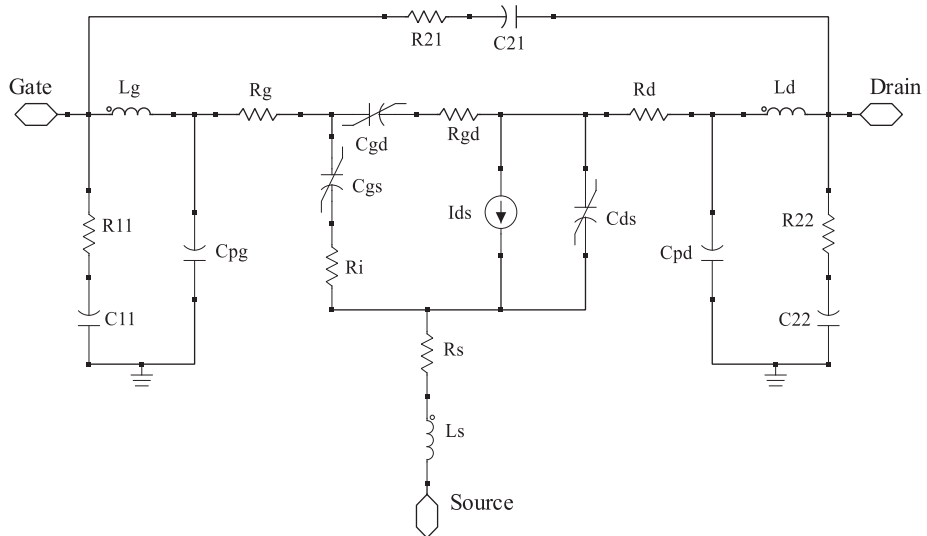
GaN HEMT CGH40045F and a GaAs FET ATF-34143, the proposed model was validated. The experimental results show an excellent correlation between the model and the measurements in all regions of the microwave FETs' I/V characteristic curve. Additionally, the proposed model can accurately determine the  $g_m$  ( $V_{GS}$ ) as well as its first and second derivatives.

The organization of the article is as follows. Section 2 describes the EEC topology and presents the proposed I/V nonlinear empirical model with the extraction procedure. Section 3 is related to the validation of the proposed model under DC and large-signal conditions. For this purpose, we made comparisons between the proposed model and the commercial model of transistors using measured data from load-pull, ACPR, and a 600 MHz class J power amplifier designed in S-band with a GaN FET CGH40010F, and we found that in all cases, the proposed model matches the measured data much better. These results demonstrate that it is essential to have an accurate  $I_{DS}$  ( $V_{GS}$ ,  $V_{DS}$ ) model to design a power amplifier. Finally, in Section 4 are presented the conclusions.

## 2 | MODEL DESCRIPTION

Figure 2 shows the EEC model of a microwave FET. The EEC has an extrinsic part represented by the parasitic elements  $R_g$ ,  $R_d$ ,  $R_s$ ,  $L_g$ ,  $L_d$ ,  $L_s$ ,  $C_{pg}$ , and  $C_{pd}$ ; these elements are bias independent. Moreover, in the GaN FETs, three R-C series networks (R11-C11, R22-C22, and R21-C21) are considered extrinsic elements.<sup>23</sup> These

**FIGURE 2** Nonlinear electrical equivalent circuit topology used



networks have been successfully adopted in References 5, 24, 25 to account for the substrate's conductivity, which affects the small-signal response.

Regarding the intrinsic part, its elements are nonlinear and bias-dependent. In that sense, the main nonlinear element of the model that contributes significantly to predicting the performance of a transistor or a microwave circuit is the drain-to-source current,  $I_{DS}(V_{GS}, V_{DS})$ , and the remaining intrinsic elements are weak nonlinearities that help to improve the accuracy of the model by modeling the FET dynamic behavior.

## 2.1 | The proposed I/V nonlinear model

The model from Reference 21, initially created for modeling the I/V characteristics of LDMOS and MOSFET devices,<sup>9,19,26</sup> has been used to model the nonlinear HEMT I/V behavior<sup>5-8,10</sup> due to its improved prediction of the nonlinear transconductance shape. Based on References 4 and 2, this work presents an empirical drain-to-source current model for HEMT GaAs and high power GaN devices.

The proposed I/V empirical model is given by

$$I_{DS}(V_{GS}, V_{DS}) = \beta_{eff} \cdot V_{gs3}^2 \cdot (1 + \lambda(V_{GS}) \cdot V_{DS}) \cdot \tanh\left(\frac{\alpha(V_{GS})}{V_{gs3}^{psat}} \cdot V_{DS}\right), \quad (1)$$

where:

$$\beta_{eff} = \frac{\beta}{1 + \mu_{crit} \cdot V_{gs3}^{g_{min}}}, \quad (2)$$

and

$$V_{gs3} = V_{ST} \cdot \ln\left(1 + e^{\left(\frac{V_{gs2}}{V_{ST}}\right)}\right), \quad (3)$$

$$V_{gs2} = V_{gs1} - \frac{1}{2} \left( V_{gs1} + \sqrt{(V_{gs1} - VK)^2 + \Delta^2} - \sqrt{VK^2 + \Delta^2} \right), \quad (4)$$

$$V_{gs1} = V_{GS} - V_{th}. \quad (5)$$

$$V_{th} = V_{th0} + \gamma \cdot V_{DS}, \quad (6)$$

$$g_{mlin} = g_{mlin0} + g_{mlinx} \cdot V_{DS}, \quad (7)$$

$$VK = VK_0 + VK_{sat} \cdot V_{DS}, \quad (8)$$

$$\lambda(V_{GS}) = \lambda_3 - \lambda_0(1 + \lambda_1 V_{GS}) \tanh(\lambda_2 V_{GS}), \quad (9)$$

$$\alpha(V_{GS}) = \alpha_0 + \alpha_1 e^{-\left(\frac{V_{GS} - \alpha_2}{\alpha_3}\right)^2}. \quad (10)$$

where  $V_{th}$ ,  $g_{mlin}$ , and  $VK$  are linear functions that depend on  $V_{DS}$ . Additionally,  $\beta$ ,  $\mu_{crit}$ ,  $V_{ST}$ ,  $\Delta$ ,  $psat$ ,  $\lambda_n$ , and  $\alpha_n$  are fitting parameters;  $V_{th0}$  is the threshold voltage for a  $V_{DS}$  close to 0 V, and  $\gamma$  is the slope of the linear dependence of  $V_{th}$  with  $V_{DS}$ .

It is worth to comment that  $g_{mlin}$  and  $VK$  are used to describe the  $V_{DS}$  dependence of  $g_m$  around its peak value and tune the slope of  $g_m$  in the linear and compression regions, respectively. To illustrate the above, let us analyze Figure 3, where is plotted the DC  $g_m$ , and it is possible to identify four operation regions (Sub-threshold, Quadratic, Linear, and Compression). When the active

device is biased in the saturation region<sup>21</sup> ( $V_{DS} > V_{knee}$ ), the  $g_m$  can be modeled using (2) and (3), and this is because (3) approaches gradually to zero in the sub-threshold region when  $V_{GS} < V_{th}$ , and the turn-on abruptness of  $g_m$ , in the quadratic region, is controlled by the parameter  $VST$ . Notice that  $g_m$  increases linearly when  $V_{GS} \gg V_{th}$ . This behavior is well described because  $V_{gs3}$  has a quasi-linear dependence with  $V_{gs2}$ , and the parameter  $\beta$  in (2) controls the slope. Moreover, the parameter  $\mu_{crit}$  in Equation (2) regulates the transition from the quadratic to the linear region. The compression region of the transconductance is tuned using function  $VK$  and parameter  $\Delta$ . They accurately represent the slow decay and elongation of the transconductance curve after achieving its maximum value (over the threshold voltage), which is the typical highly asymmetrical bell-shaped form of the transconductance when the transistor is biased in the saturation region. This set of equations allows a continuous and smoother transition in the derivative of  $I_{DS}$  as a function of  $V_{GS}$ .

Furthermore, the addition of sub-threshold conduction in Equation (3) is critical to avoid a discontinuity in the drain current expression derivatives at  $V_{GS} = V_{th}$ .<sup>26</sup>

In contrast with the device models presented in References 3 and 16 for GaN FETs, in Reference 21 for LDMOS or Reference 20 for MESFET devices, the empirical formulation for  $I_{DS}(V_{GS}, V_{DS})$  presented in this article accurately represents the nonlinear transconductance shape and its transitions for all values of  $V_{DS}$ . This fact is not only for the highly asymmetrical bell-shaped form of the transconductance (already analyzed and modeled<sup>5,11</sup>), but also for the quasi-symmetrical bell-shaped form obtained when the device is biased with a  $V_{DS}$  in the ohmic region of the  $I_{DS} - V_{DS}$  characteristic<sup>22</sup> as seen in Figure 4, where a comparison between measured and

modeled  $g_m$  using Reference 21, and our proposed model, at low  $V_{DS}$  values obtained from pulsed measurement of the GaN FET CGH40045F, are plotted. The results demonstrate that the model of Reference 21 is unable to follow the transconductance behavior accurately, and hence its correlation with the measurement is low.

Finally, we want to highlight the main features of the proposed model inspired by the models of References 2 and 4:

1. To the best of the author's knowledge, Equation (7) is new. This equation, along with (8), allows us to accurately determine the maximum transconductance value and its shaping around this value, considering the transconductance's nonlinear behavior as  $V_{DS}$  changes.
2. Gate-to-source voltage dependence of the output conductance. This dependency is considered by Equation (9), which allows us to model the drain-to-source current at large  $V_{DS}$  values, especially when the  $V_{GS}$  voltage is close to  $V_{th}$ .
3. Function (10) is useful in reproducing the displacement of the knee voltage ( $V_{knee}$ ) in the  $I_{DS} - V_{DS}$  curves and modeling the subtle complexities in the ohmic region for different active devices. Moreover, it is important to comment that (10) directly influences the improved performance achieved in the transconductance modeling for low values of  $V_{DS}$ , as shown in Figure 4. In fact, in our proposed model, we adopted the term  $V_{gs3}^{psat}$  in Equation (1) instead of the  $\tanh(\alpha(V_{GS}) \cdot V_{DS})$  as proposed in Reference 4. This modification allows the drain saturation current to depend on the gate to source voltage, which causes the transconductance to decrease after the saturation point has been reached, likewise improves the fitting of the data in the ohmic region.

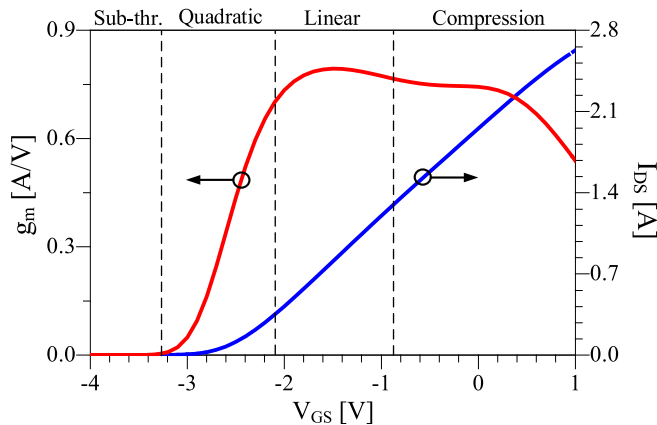


**FIGURE 3** Transconductance regions and drain current for a GaN HEMT CGH40010F at  $V_{GSq} = -2.5$  V and  $V_{DSq} = 28$  V, with a  $V_{DS}$  biased in the saturated region

## 2.2 | Extraction procedure of initial values

The proposed model's initial values are determined using the experimental I/V data, such as parameters  $V_{th}$ ,  $V_{th0}$ , and  $\gamma$ . Parameter  $VST$  can be determined as follows<sup>9</sup>:

$$VST = \frac{I_{th}}{\ln(2)}, \quad (11)$$

where  $I_{th}$  is the threshold current at  $V_{GS} = V_{th}$ , extracted at a  $V_{DS}$  value close to 0 V.

Coefficient  $\mu_{crit}$  can be assigned as  $0.5 \text{ V}^{-1}$ , whereas coefficient  $psat$  can take an initial value close to one. Fitting parameters  $g_{mlin0}$ ,  $g_{mlinx}$ ,  $VK_0$ ,  $VK_{sat}$ , and  $\Delta$  can be

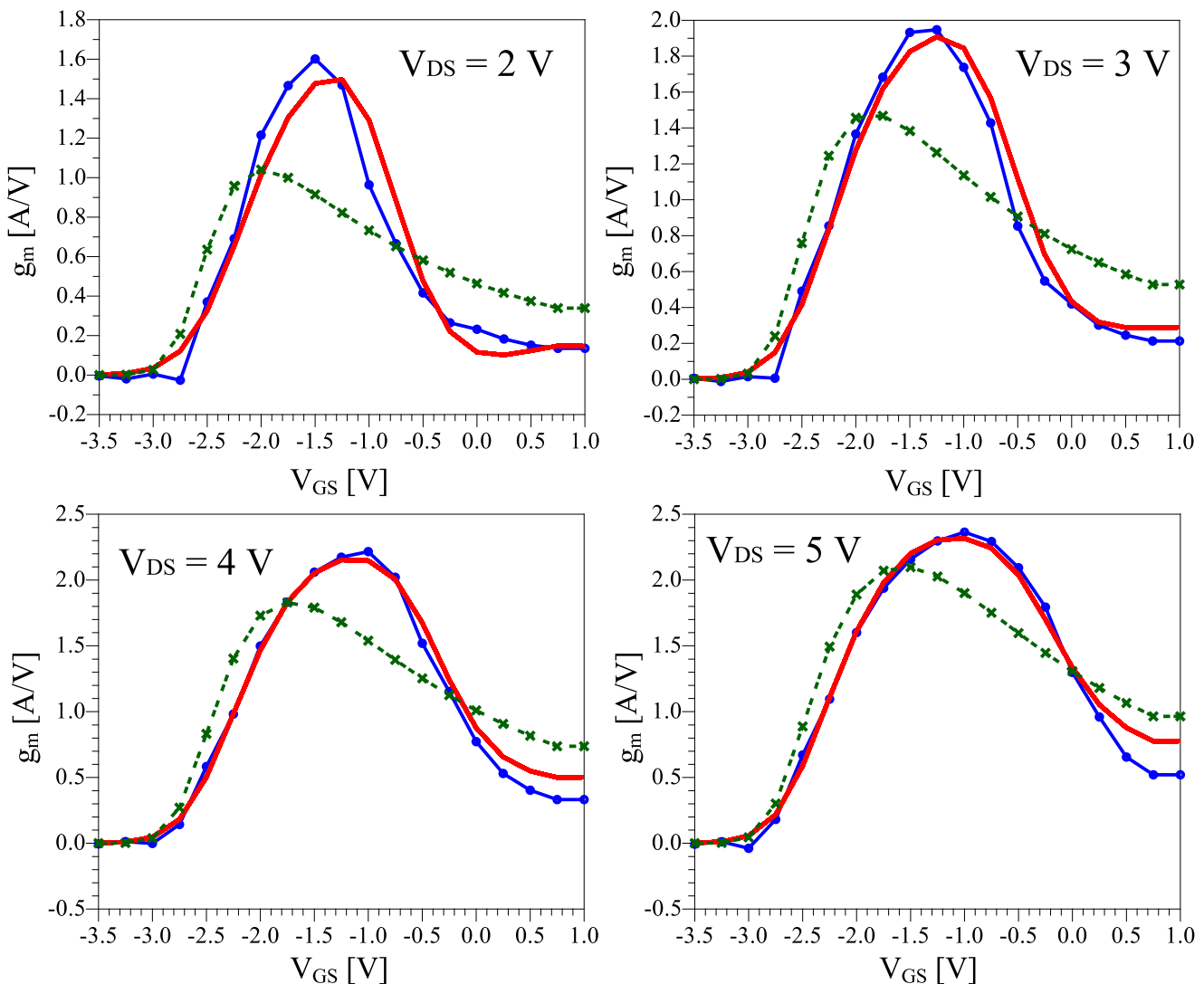


**FIGURE 4** Comparison of measured (circles) and modeled transconductance using the proposed model (solid lines), and the model from Reference 21 ( $\times$ ), for the GaN CGH40045F at  $V_{G Sq} = -2.5$  V and  $V_{D Sq} = 28$  V, illustrating the quasi-symmetrical bell-shaped characteristic of the transconductance at  $V_{DS}$  values inside the ohmic region of the  $I_{DS} - V_{DS}$  characteristic

determined by numerical optimization. On the other hand, coefficient  $\beta$  can be fitted with reasonable accuracy by numerical experiments since this parameter has a well-defined meaning in terms of its influence on the shape of  $g_m$ .

Regarding the extraction of parameters in Equations (9) and (10), the output conductance ( $\lambda$ ) is determined from the slope of the  $I_{DS} - V_{DS}$  characteristic at a saturated channel condition, and the saturation voltage ( $\alpha$ ) is 25% of the knee voltage.<sup>13</sup> Thus,  $\lambda$  and  $\alpha$ , in the proposed model, are determined for all  $V_{GS}$  values greater than the pinch-off voltage following the above criteria. The result of these operations is a set of points of  $\lambda(V_{GS})$  and  $\alpha(V_{GS})$ , one for each  $V_{GS}$  value, as shown in Figure 5. Once  $\lambda(V_{GS})$  and  $\alpha(V_{GS})$  are known, the parameters  $\lambda_n$  ( $n = 0, 1, 2, 3$ ) and  $\alpha_n$  ( $n = 0, 1, 2, 3$ )

from Equations (9) and (10), respectively, are determined using the curve fitting toolbox from MATLAB and employing a nonlinear least-square optimization method.

### 3 | EXPERIMENTAL RESULTS

Three packaged active devices (two GaN HEMTs from Wolfspeed, CGH40010F and CGH40045F, and a GaAs ATF-34143) were measured and characterized under different operation conditions to validate the proposed model. The three packaged transistors' experimental I/V data were measured using the pulsed I/V system Auriga AU4950 configured with a pulse width of 4, 0.5, and 5  $\mu$ s for the packaged GaN HEMT CGH40045F, CGH40010F,

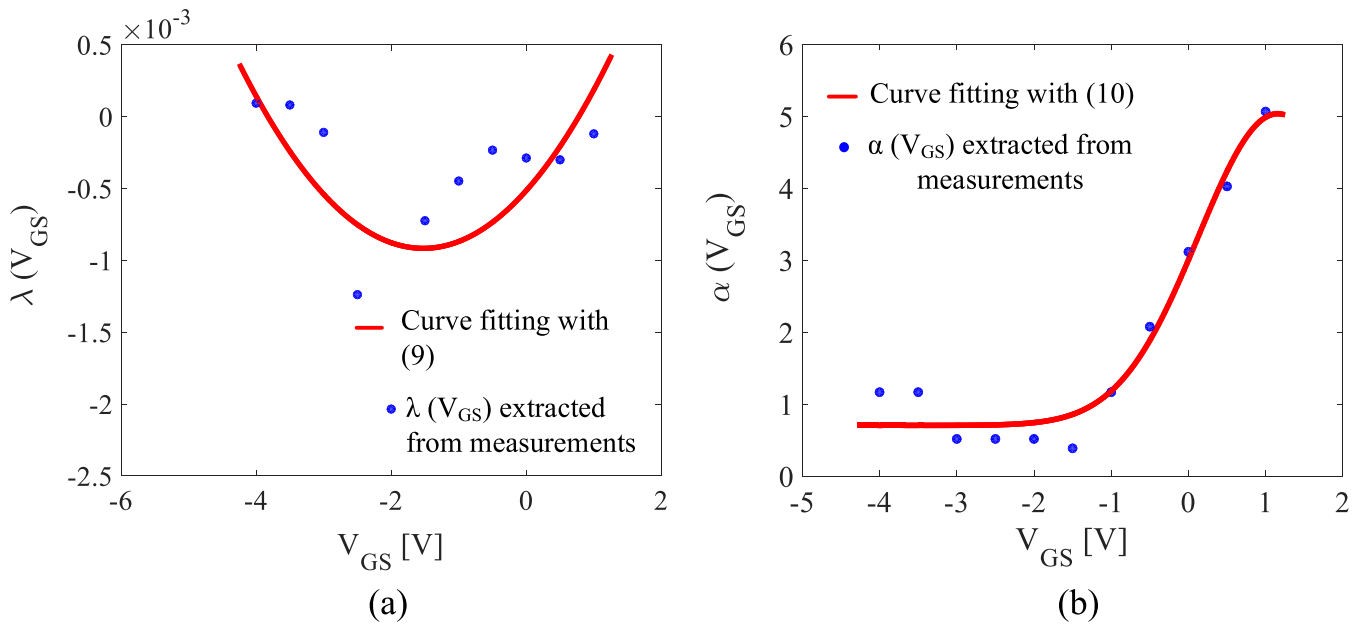


**FIGURE 5** Curve fitting analysis of functions  $\lambda(V_{GS})$  and  $\alpha(V_{GS})$  for the GaN CGH40045F employing the curve fitting toolbox of MATLAB with Equations (9) and (10)

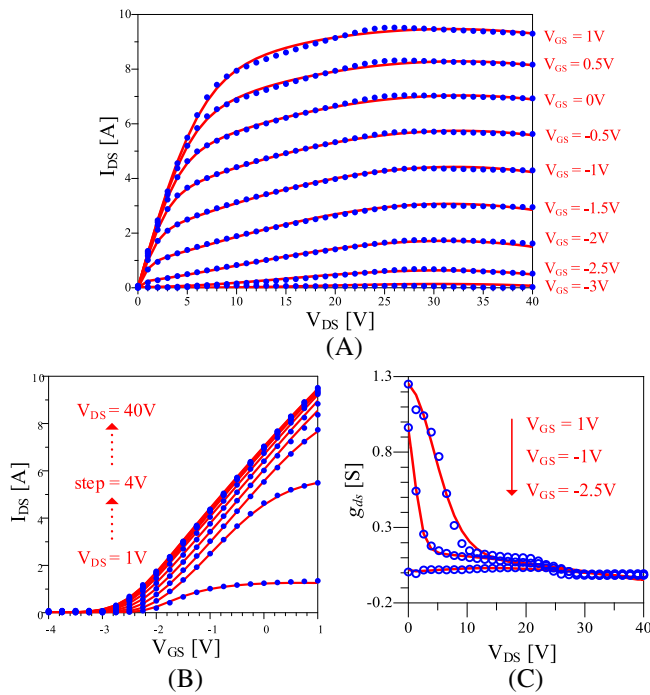


**FIGURE 6** Comparison of measured (circle) and simulated data using the proposed model (solid line), for a packaged GaN HEMT CGH40045F. (A)  $I_{DS}$  –  $V_{DS}$ , (B)  $I_{DS}$  –  $V_{GS}$ , and (C) output conductance, at a  $V_{GSq} = -2.5$  V and  $V_{DSq} = 28$  V. Nonquiescent drain voltage was swept from  $V_{DS} = 0$  V to  $V_{DS} = 40$  V with steps of 1 V, and the nonquiescent gate voltage was swept from  $V_{GS} = -4$  V to  $V_{GS} = 1$  V with steps of 0.5 V

**TABLE 1** Model parameter values for the CGH40045F

VST (V)	$\mu_{crit}$ (V <sup>-1</sup> )	g <sub>mlin0</sub>	V <sub>K0</sub> (V)	V <sub>tho</sub> (V)
0.25	0.26	1.692	0.04681	-2.377
$\gamma$	$\beta$ (1/Ω)	g <sub>mlin0</sub> (V <sup>-1</sup> )	V <sub>Ksat</sub>	psat
-0.04027	1.78555	0.01463	5.306	0.62249
$\lambda_0$ (1/V)	$\lambda_1$ (1/V)	$\lambda_2$ (1/V)	$\lambda_3$ (1/V)	$\Delta$ (V)
-1.98237	-0.006269	0.0072705	0.0174368	13.2896
$\alpha_0$ (1/V)	$\alpha_1$ (1/V)	$\alpha_2$ (V)	$\alpha_3$ (V)	
0.657506	3.75704	-3.06779	-1.82375	

and the pseudomorphic HEMT ATF-34143, respectively. Each active device was biased as follows; for the CGH40010F a  $V_{GSq} = -2.8$  V and  $V_{DSq} = 28$  V, for the CGH40045F a  $V_{GSq} = -2.5$  V and  $V_{DSq} = 28$  V, and finally for the ATF34143 a  $V_{GSq} = -0.54$  V and  $V_{DSq} = 2$  V.

On the other hand, S-parameters measured with a calibrated<sup>27</sup> PNA-X N5242A from 0.4 to 4.0 GHz were used to extract the devices' extrinsic and intrinsic elements. In that sense, the first step was to obtain the R-C series networks (R11-C11, R22-C22, and R21-C21) from the admittance parameters of an open dummy structure.<sup>25,28</sup> Considering that the number of parasitic elements surpasses the number of equations representing the real and imaginary parts of the admittance

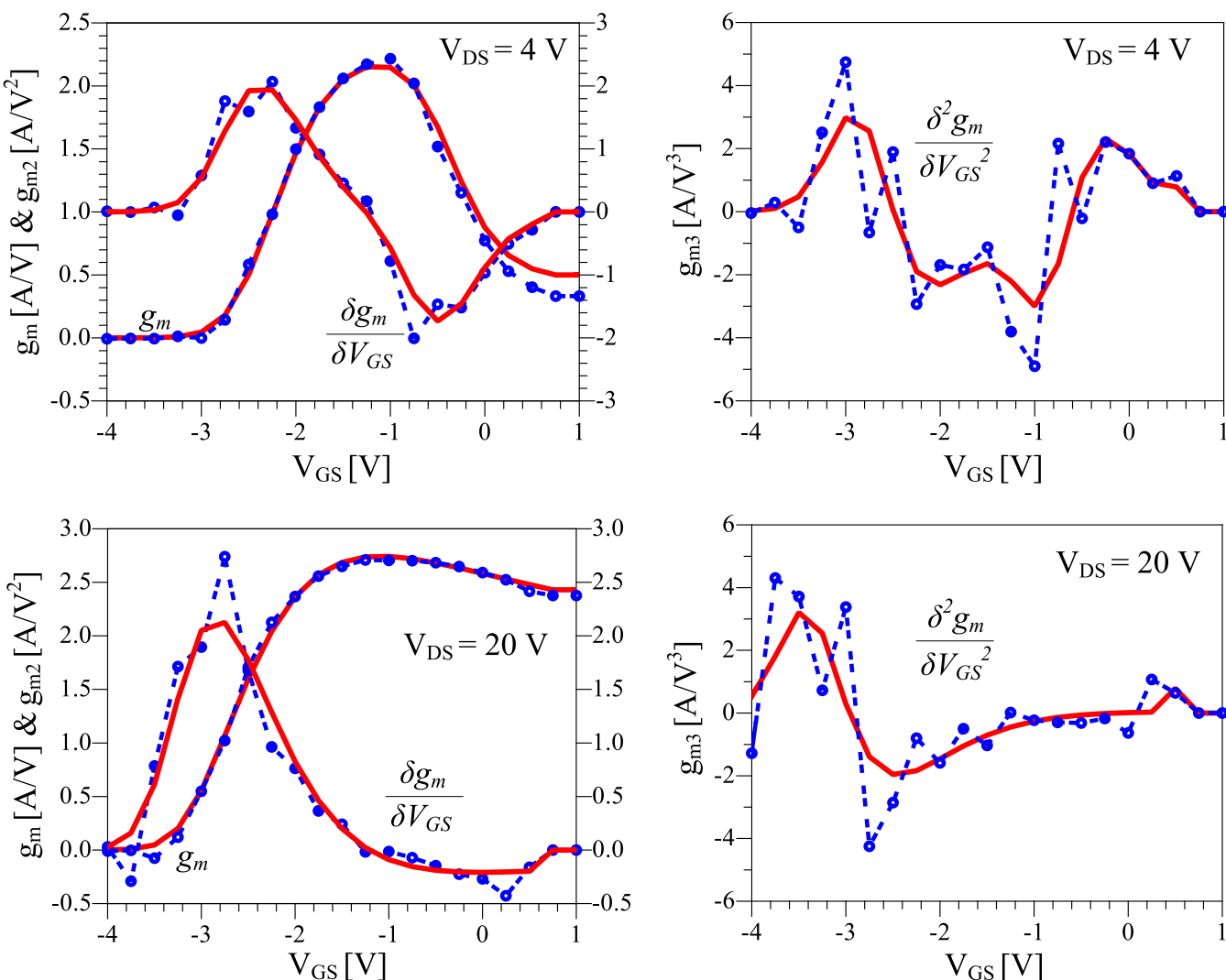


**FIGURE 7** Comparison of measured (circles) and modeled transconductance and its first and second derivatives using the proposed model (solid lines) for the GaN CGH40045F. At a  $V_{GSq} = -2.5\text{ V}$  and  $V_{DSq} = 28\text{ V}$ , illustrating the transconductance accurate representation at  $V_{DS} = 4\text{ V}$  (top) and  $V_{DS} = 20\text{ V}$  (below)

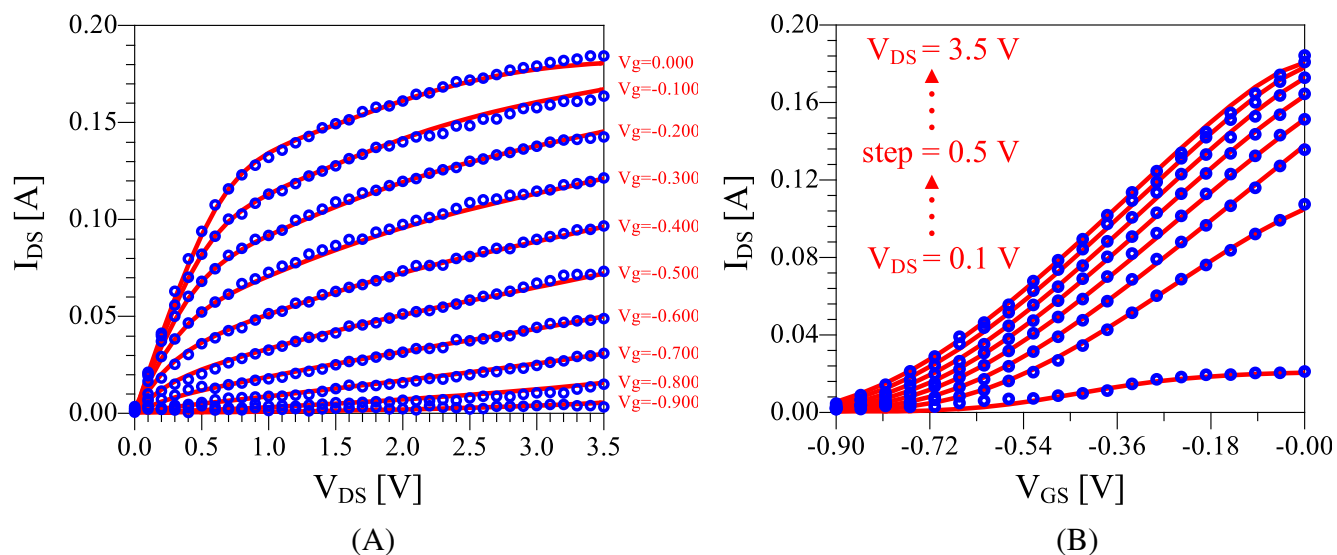


**FIGURE 8** Comparison of measured (circles) and modeled drain-to-source current using the proposed model (solid lines) with  $V_{GSq} = -0.54\text{ V}$  and  $V_{DSq} = 2\text{ V}$ , for the GaAs ATF34143. (A)  $I_{DS} - V_{DS}$  and (B)  $I_{DS} - V_{GS}$

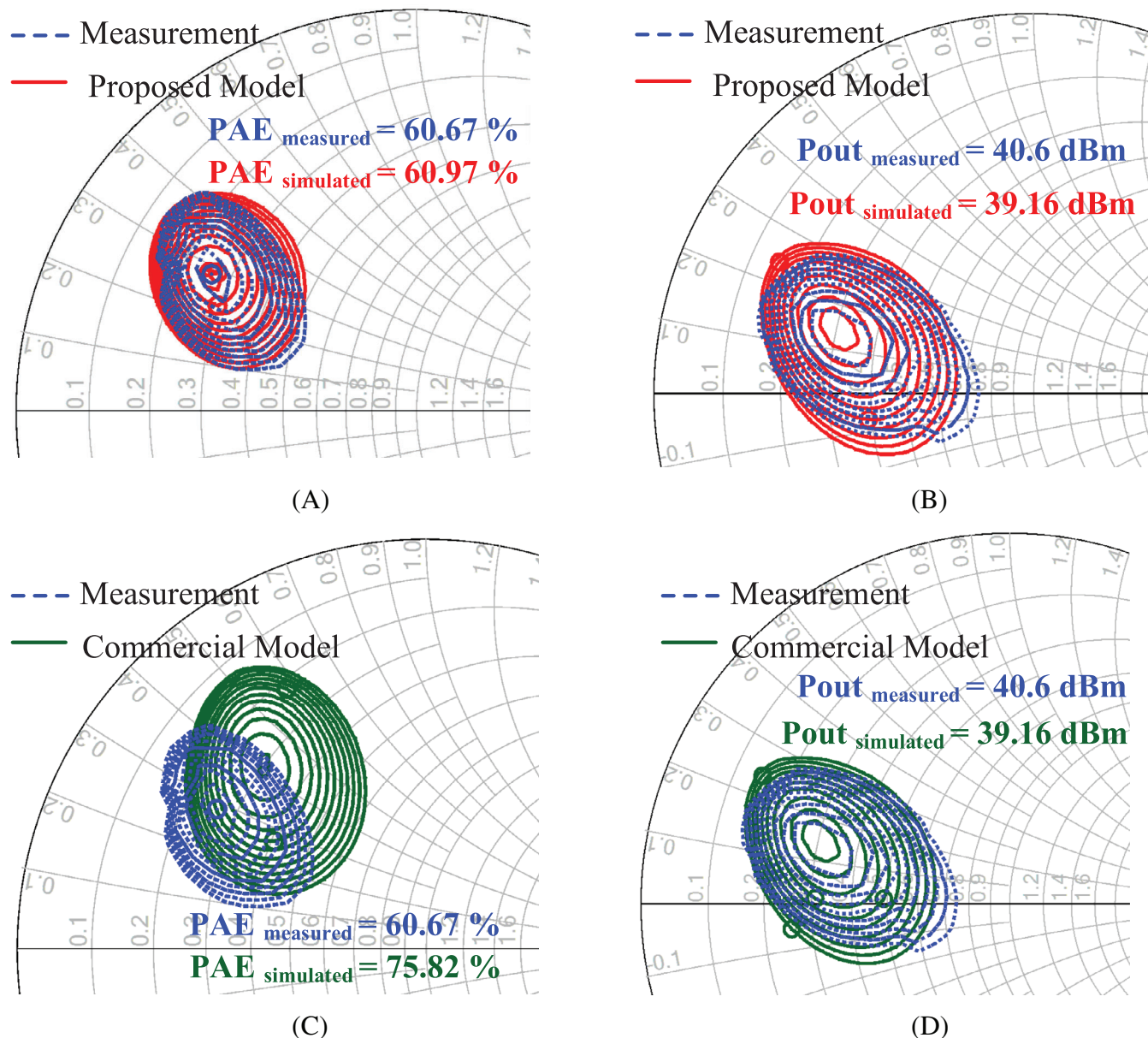


**FIGURE 9** Comparison of load-pull PAE and  $P_{\text{out}}$  contours at 2 GHz with an input power of 31 dBm for the HEMT CGH40010F, at a  $V_{\text{GSq}} = -2.8$  V and  $V_{\text{DSq}} = 28$  V. Measured data (dot) and simulated with the proposed model (solid line) (A,B), and with the commercial model (solid line), (C,D)

parameters, an optimization was done using the commercial CAD tool Advance Design System (ADS) to obtain these six elements.<sup>24,28</sup> Afterward, biasing the transistors under forward and reverse Cold-FET conditions, as suggested in References 29–31, the extrinsic elements were extracted. After de-embedding the extrinsic elements from hot S-parameters measurements, using a similar procedure described by References 32, 33, the intrinsic elements were determined using the method reported in Reference 34.

The EEC (see Figure 2) considering the proposed I/V model is easy to implement in the microwave circuit

simulator ADS using the SDD component. It is worth commenting that thermal effects and traps are not considered in this work. Besides, the I/V pulsed data are not isodynamic I/V<sup>35, 36</sup> because we currently do not have a test bench for making these measurements. However, our main interest is to highlight the importance of an accurate I/V model for designing microwave circuits like power amplifiers, even when it does not consider the thermal or traps effects. In that sense, we will compare simulation results using our proposed model with the transistors' commercial models under different large-signal tests.

### 3.1 | DC validation of the proposed model

The I/V models developed for the packaged GaN FETs CGH40010F, CGH40045F, and the GaAs FET ATF34143 use pulsed I/V measured data for mitigating self-heating and trapping conditions. In the CGH40010F and ATF34143, the quiescent gate voltage was set to less than the pinch-off voltage. Therefore, the devices dissipate no power and, consequently, are free of any static self-heating conditions.<sup>11</sup> However, in the GaN CGH40045F, the quiescent gate voltage was a bias point where the transistor is in conduction, as a class AB, and therefore it presents a prominent kink effect when compared with the other two transistors.

Figure 6 compares the measured and modeled data of the intrinsic  $I_{DS} - V_{DS}$ ,  $I_{DS} - V_{GS}$ , and the output conductance for the packaged HEMT CGH40045F, whereas in Table 1 are reported the values of the fitting parameters. Notice the excellent fitting of the proposed model with the measured data compared with the simulation results using the model from Reference 21 (see Figure 1). These results demonstrate the proposed model's versatility for modeling atypical behaviors on the FET's I/V curves. Moreover, Figure 7 shows measured and modeled  $g_m$  data and its first and second derivatives ( $g_{m2}$  and  $g_{m3}$ ), where the relative error is less than 10% with our proposed model.

Besides, Figure 8 shows the comparison results between measured and modeled data of the intrinsic  $I_{DS} - V_{DS}$  and  $I_{DS} - V_{GS}$  for the GaAs ATF34143; also, a high degree of precision is achieved resulting from using the proposed  $I_{DS}(V_{GS}, V_{DS})$  model.

In practice, the measured pulsed I/V curves depend on the quiescent point, particularly with  $V_{GS}$ . In some cases, depending on each particular FET, the slope of the I/V curves in the ohmic and saturation regions can change significantly. In that sense, it is important to

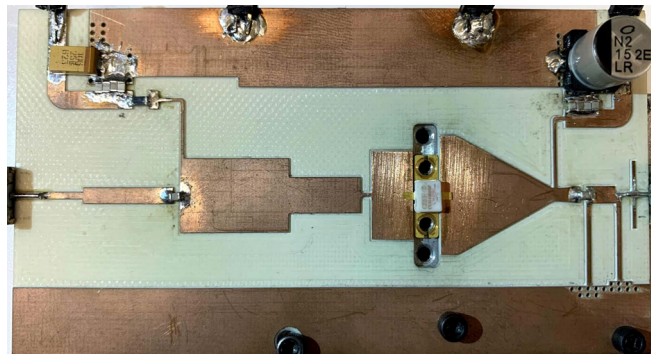


**FIGURE 10** Photograph of the implemented class-J PA using a HEMT CGH40010F

comment that in the proposed model, these changes can be considered by tuning the variables  $\alpha_n$ ,  $VST$ ,  $V_{th0}$ ,  $psat$ , and  $\gamma$  for the ohmic region; and  $\lambda_n$  for the saturation region. This feature helps to quickly model the pulsed I/V characteristics at a different quiescent point of the same FET.

### 3.2 | GaN HEMT CGH40010F: load-pull measurements and broadband high efficiency Class-J PA design

Now the proposed model is validated under large-signal conditions. For this purpose, the output power ( $P_{out}$ ) and power added efficiency (PAE) contours of the GaN

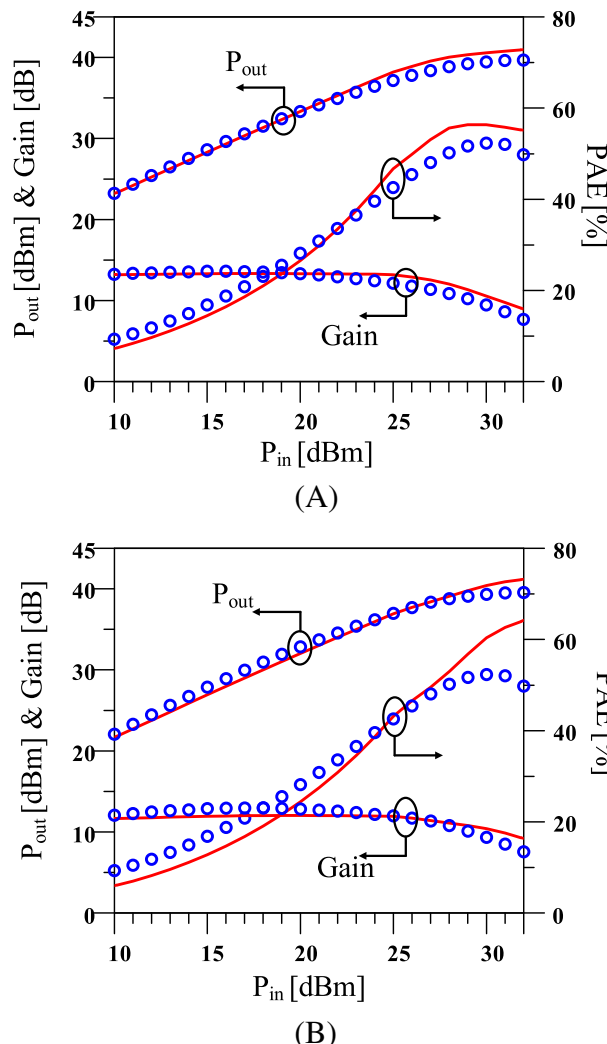


**FIGURE 11** Comparison of measured (circles) and simulated (solid line)  $P_{out}$ , PAE and Gain vs input power for the class-J PA designed using the proposed model under CW operation, for (A) 3 GHz and (B) 3.6 GHz.  $V_{GSq} = -2.8$  V and  $V_{DSq} = 28$  V

HEMT CGH40010F were measured using an impedance tuner i1818 from Focus Microwaves.

Figure 9 shows the load-pull contours; these contours correspond to 2 GHz with an input power of 31 dBm and biased with quiescent voltages of  $V_{DSq} = 28$  V and  $V_{GSq} = -2.8$  V (class-B operation). Notice that the simulated contours with the proposed model, Figure 9A,B, can predict the behavior of the GaN CGH40010F very well, where the maximum simulated PAE has an absolute error of 0.3%, and the absolute error for the maximum power prediction is 1.4 dB. On the other hand, Figure 9C,D shows the simulated load-pull contours results using the nonlinear commercial model, where the user cannot access or modify the model's equations. Notice that although the commercial model contains parasitic elements, nonlinear intrinsic elements, and thermal/charge trapping models, the PAE contours prediction is highly inaccurate. It is worth to comment that we also compared the simulated Load-Pull data using the model of Reference 21, and the results are slightly different from our model. This fact was expected as both models fit very well in the transistor's I/V curves' saturation region. However, for applications other than designing an amplifier such as designing a low distortion mixer,<sup>37</sup> our proposed model is likely more suitable since in the latter case the I/V model has to fit very well in the ohmic region.

Furthermore, we designed a broadband high-efficiency class-J PA with the aid of the proposed model. The designed class-J PA, biased with  $V_{DS} = 28$  V and  $V_{GS} = -2.8$  V, operates in the S-band (3 GHz). The input

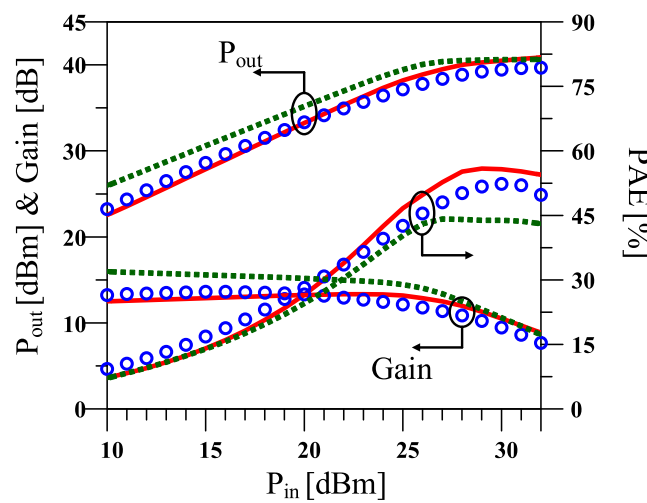


**FIGURE 12** Comparison of measured (circle), simulated with the commercial model (discontinuous line) and simulated with the proposed model (solid line)  $P_{out}$ , PAE and Gain vs input power for the designed class-J PA under 3 GHz CW operation, at a  $V_{GSq} = -2.8$  V and  $V_{DSq} = 28$  V

and output matching networks were designed based on the characteristics of the Rogers high-frequency laminate RO4003C with  $\epsilon_r = 3.55$ . Figure 10 shows a photograph of the fabricated power amplifier.

Figure 11 compares the class-J PA simulation results using the proposed model with measured data of  $P_{out}$ , PAE, and gain under CW operation at two different frequencies, 3 and 3.6 GHz. The experimental results show a class-J PA with a maximum  $P_{out}$  and PAE of 10 W and 52%, respectively, with an associated gain of approximately 8 dB for the two frequencies. Notice the high correlation between the simulated and measured data of the  $P_{out}$  and gain, using the proposed model, where errors less than 1 dB are observed. Regarding the PAE

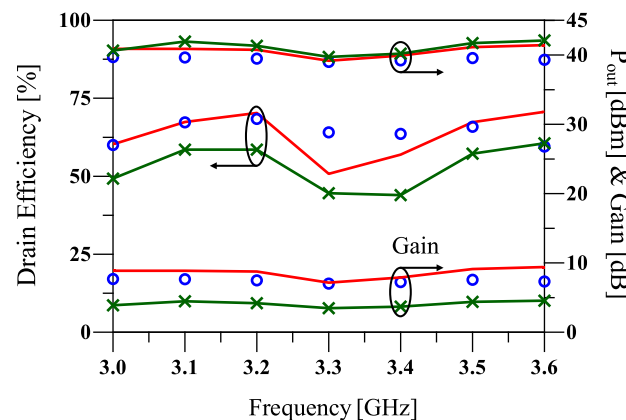


**FIGURE 13** Comparison of measured (circle), simulated with the commercial model (x) and simulated with the proposed model (solid line)  $P_{out}$ , Gain and Drain Efficiency vs frequency for the designed class-J PA with an input power of 32 dBm, at a  $V_{GSq} = -2.8$  V and  $V_{DSq} = 28$  V

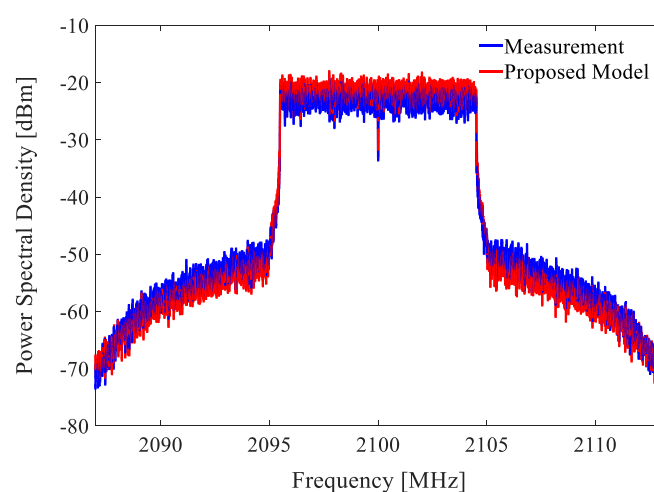


**FIGURE 14** Comparison of measured and simulated, with the proposed model, output power spectra using a 10 MHz bandwidth LTE signal with  $V_{GSq} = -0.54$  V,  $V_{DSq} = 2$  V and  $P_{in} = -2$  dBm

**TABLE 2** Measured and simulated results for the GaAs HEMT ATF-34143 under digital modulated stimulus

$V_{GS}$ (V)	$V_{DS}$ (V)	$P_{in}$ (dBm)	$P_{out}$ (dBm)			ACPR-L (dBc)			ACPR-U (dBc)		
			Meas.	Sim.	Comm.	Meas.	Sim.	Comm.	Meas.	Sim.	Comm.
-0.54	2	-4	8.06	9.28	11.03	-38.1	-41.7	-30.7	-37.87	-41.8	-30.64
-0.54	2	-2	9.81	11.1	12.87	-32.57	-34.8	-28.48	-32.48	-35.01	-28.54
-0.8	2	-2	7.3	10.1	12.94	-32.92	-35.55	-28.37	-33.58	-36.36	-28.44

Note: Sim. and Comm. correspond to simulated results using the proposed model and the commercial model, respectively.

simulation, it deviates slightly from the measurements. In the worst case, there is a difference of 10%. Nevertheless, compared with simulation results using the nonlinear commercial model at 3 GHz, the proposed model predicts the  $P_{out}$ , PAE, and gain accurately, as shown in Figure 12.

Moreover, Figure 13 shows the measured and simulated  $P_{out}$ , drain efficiency, and gain results in the frequency band of 3 to 3.6 GHz. Good agreement between measurement and simulation with the proposed model was achieved, not being the case when using the commercial model.

### 3.3 | GaAs HEMT ATF34143: intermodulation distortion

Finally, we compared the simulated and measured ACPR-generated from a pseudomorphic GaAs HEMT ATF-34143, using an LTE signal with 10 MHz of bandwidth, 7 dB of PAPR, and centered at a frequency of 2.1 GHz. The ACPR was measured using a vector signal generator (MXG N5182A) and a digital signal analyzer (DSA90404A), both controlled by the VSA software, and with the aid of ADS was obtained the output power spectrum. Figure 14 shows the measured and simulated output spectrum, where it is remarkable the excellent correlation between the simulation and the measurement. Table 2 reports the measured and simulated data, using the proposed and commercial models, of the output power and ACPR at different input power levels and bias points. An error of less than 1.3 dB is observed in  $P_{out}$ , and in the case of the ACPR, the maximum error is 3.93 dB when using the proposed model, which is not the case when using the commercial model where the error predicting the  $P_{out}$  ascend to 3 dB and the ACPR error to 7.4 dB. These results demonstrate that an accurate I/V model is the most critical nonlinear element to consider in the EEC of microwave FETs; this allows us to get a good approximation of the principal figures of merit of the power amplifier.

## 4 | CONCLUSIONS

An improved nonlinear empirical I/V model suitable for modeling the drain-to-source current of GaAs and GaN FETs has been presented. The proposed model introduces modifications to an LDMOS behavioral equations, allowing us to consider the output conductance and saturation voltage dependence with  $V_{GS}$ . Moreover, the proposed model is able to describe the highly nonlinear shape of the transconductance for all  $V_{DS}$  values. That is possible, thanks to a new function that considers the dependence of  $V_{DS}$  in the linear region of the transconductance. Furthermore, with the proposed model, GaN, and GaAs HEMTs may be modeled from the ohmic to the saturation region, including the pinch-off region and the first and second derivatives of the transconductance. A microwave FET model that consists of package parasitic, linear extrinsic, and bias-invariant intrinsic elements, along with the proposed I/V model, has demonstrated the capacity to represent the behavior under large-signal excitation of GaAs and GaN transistors. Load-Pull and ACPR measurements data at different frequencies validate the proposed model. Furthermore, data measurements of a class-J PA designed at S-band frequencies with 600 MHz of bandwidth were used, demonstrating the proposed model's usefulness to simulate microwave power amplifiers.

## ACKNOWLEDGMENT

This work was supported by the National Council of Science and Technology of Mexico (CONACyT) under projects number 163272 and 206029 and the students' scholarships involved in this work. Furthermore, the authors also want to thank the anonymous reviewers for their thoughtful revision and keen observation.

## DATA AVAILABILITY STATEMENT

The data that support the findings of this study are available from the corresponding author upon reasonable request.

**ORCID**

Daniel Ochoa-Armas  <https://orcid.org/0000-0003-3692-550X>

Ismary Lavandera-Hernández  <https://orcid.org/0000-0002-0681-414X>

José R. Loo-Yau  <https://orcid.org/0000-0001-7467-2537>  
Cain Pérez-Wences  <https://orcid.org/0000-0003-0682-5364>

J. Apolinar Reynoso-Hernández  <https://orcid.org/0000-0003-4131-4981>

**REFERENCES**

1. Pedro JC, De Carvalho NB. *Intermodulation Distortion in Microwave and Wireless Circuits*, Boston. Artech House: Norwood; 2003:199-235.
2. De Carvalho NB, Pedro JC. Large- and small-signal IMD behavior of microwave power amplifiers. *IEEE Trans Microw Theory Techn.* 1999;47(12):2364-2374. <https://doi.org/10.1109/22.808983>.
3. Angelov I, Zirath H, Rosman N. A new empirical nonlinear model for HEMT and MESFET devices. *IEEE Trans Microw Theory Tech.* 1992;40(12):2258-2266. <https://doi.org/10.1109/22.179888>.
4. García-Osorio A, Loo-Yau JR, Reynoso-Hernández JA, Ortega CS, Valle-Padilla JLD. An empirical I-V nonlinear model suitable for GaN FET class F PA design. *Microw Opt Technol Lett.* 2011;53(6):1256-1259. <https://doi.org/10.1002/mop.25980>.
5. Cabral P, Pedro J, Carvalho N. Nonlinear device model of microwave power GaN HEMTs for high power-amplifier design. *IEEE Trans Microw Theory Tech.* 2004;52(11):2585-2592. <https://doi.org/10.1109/tmtt.2004.837196>.
6. Khawam Y, Albasha L. Extended behavioral modelling of FET and lattice-mismatched HEMT devices. *Int J Electron.* 2017;104(7):1228-1237. <https://doi.org/10.1080/00207217.2017.1293171>.
7. Jarndal A, Ghannouchi FM. Improved modeling of GaN HEMTs for predicting thermal and trapping-induced-kink effects. *Solid-State Electron.* 2016;123:19-25. <https://doi.org/10.1016/j.sse.2016.05.015>.
8. Prasad A, Thorsell M, Zirath H, Fager C. Accurate modeling of GaN HEMT RF behavior using an effective trapping potential. *IEEE Trans Microw Theory Techn.* 2018;66(2):845-857. <https://doi.org/10.1109/tmtt.2017.2748950>.
9. Grebennikov AV, Lin F. An efficient CAD-oriented large-signal MOSFET model. *IEEE Trans Microw Theory Techn.* 2000;48(10):1732-1742. <https://doi.org/10.1109/22.873903>.
10. Prasad A, Thorsell M, Yhland K, Fager C. Symmetry based nonlinear model for GaN HEMTs. 2015 10th European Microwave Integrated Circuits Conference (EuMIC), Paris, France; 2015. <https://doi.org/10.1109/eumic.2015.7345074>.
11. Yuk KS, Branner GR, McQuate DJ. A wideband multiharmonic empirical large-signal model for high-power GaN HEMTs with self-heating and charge-trapping effects. *IEEE Trans Microw Theory Techn.* 2009;57(12):3322-3332. <https://doi.org/10.1109/tmtt.2009.2033299>.
12. Statz H, Newman P, Smith IW, Pucel RA, Haus HA. GaAs FET device and circuit simulation in SPICE. *IEEE Trans Electron Dev.* 1987;34(2):160-169. <https://doi.org/10.1109/T-ED.1987.22902>.
13. Chen YC, Ingram DL, Yen HC, Lai R, Streit DC. A new empirical I-V model for HEMT devices. *IEEE Microw Guided Wave Lett.* 1998;8(10):342-344. <https://doi.org/10.1109/75.735415.a>.
14. Tanimoto T. Analytical nonlinear HEMT model for large signal circuit simulation. *IEEE Trans Microw Theory Techn.* 1996;44(9):1584-1586. <https://doi.org/10.1109/22.536608>.
15. Liu LS. Enhanced prediction of GaN MISHEMT RF power performance using improved large-signal model. *Electron Lett.* 2011;47(7):447. <https://doi.org/10.1049/el.2010.3687>.
16. Angelov I, Desmaris V, Dynefors K, Nilsson PA, Rorsman N, Zirath H. On the large-signal modelling of AlGaN/GaN HEMTs and SiC MESFETs. Proceedings of European Gallium Arsenide and Other Semiconductor Application Symposium, GAAS 2005, Paris, France; 2005:309-312.
17. Li M-J, Li Z, Wang L-L. A novel artificial neural network-based nonlinear output current model for GaAs pHEMT with accurate high-order derivatives. *Int J Numer Model El.* 2020;33: e2736. <https://doi.org/10.1002/jnm.2736>.
18. Xu J, Yagoub MCE, Ding R, et al. Exact adjoint sensitivity analysis for neural-based microwave modeling and design. *IEEE Trans Microw Theory Techn.* 2003;51(1):226-237.
19. Motorola's Electro Thermal (MET) LDMOS Model. [https://www.nxp.com/files-static/abstract/ldmos\\_models/MET\\_LDMOS\\_MODEL\\_DOCUMENT\\_1001.pdf](https://www.nxp.com/files-static/abstract/ldmos_models/MET_LDMOS_MODEL_DOCUMENT_1001.pdf). Accessed March 2, 2020.
20. Yuk KS, Branner GR. An empirical large-signal model for SiC MESFETs with self-heating thermal model. *IEEE Trans Microw Theory Techn.* 2008;56(11):2671-2680.
21. Fager C, Pedro J, Carvalho ND, Zirath H. Prediction of IMD in LDMOS transistor amplifiers using a new large-signal model. *IEEE Trans Microw Theory Techn.* 2002;50(12):2834-2842. <https://doi.org/10.1109/tmtt.2002.805187>.
22. Chen C-H, Sadler R, Wang D, et al. The causes of GaN HEMT bell-shaped transconductance degradation. *Solid-State Electron.* 2016;126:115-124. <https://doi.org/10.1016/j.sse.2016.09.005>.
23. Chumbes EM, Schremer AT, Smart JA, et al. AlGaN/GaN high electron mobility transistors on Si(111) substrates. *IEEE Trans Electron Devices.* 2001;48(3):420-426. <https://doi.org/10.1109/16.906430>.
24. Manohar S, Narayanan A, Keerti A, Pham A, Brown J, Borges R, Linthicum K. Characteristics of microwave power GaN HEMTs on 4-inch Si wafers. 2002 IEEE MTT-S International Microwave Symposium Digest Vol. 1, Seattle, WA; 2002: 449-452. <https://doi.org/10.1109/mwsym.2002.1011652>.
25. Xiao D, Schreurs D, De Raedt W, Derluyn J, Germain M, Nauwelaers B, Borghs G. A new method to characterize substrate conductivity. 2007 70th ARFTG Microwave Measurement Conference (ARFTG), Tempe, AZ; 2007:1-4. <https://doi.org/10.1109/arftg.2007.8376180>.
26. Miller M, Dinh T, Shumate E. A new empirical large signal model for silicon RF LDMOS FETs. IEEE MTT-S Symposium on Technologies for Wireless Applications Digest, Vancouver, BC, Canada; 1997:19-22. <https://doi.org/10.1109/mttwa.1997.595103>.
27. Reynoso-Hernández, JA, Pulido-Gaytan, MA, Zarate-de Landa, A., Zuniga-Juarez, JE, Monjardin-Lopez, JR, Garcia-Osorio, A, Orozco-Navarro D, Loo-Yau JR, Maya-Sanchez, MC. Using lines of arbitrary impedance as standards on the TRL calibration technique. 81st ARFTG Microwave Measurement Conference, Seattle, WA; 2003:1-4. <https://doi.org/10.1109/arftg.2013.6579059>.
28. Crupi G, Xiao D, Schreurs DMM-P, et al. Accurate multibias equivalent-circuit extraction for GaN HEMTs. *IEEE Trans*

- Microw Theory Techn.* 2006;54(10):3616-3622. <https://doi.org/10.1109/tmtt.2006.882403>.
29. Landa AZ-D, Zuniga-Juarez J, Loo-Yau JR, Reynoso-Hernández J, Maya-Sánchez M, Valle-Padilla JD. Advances in linear modeling of microwave transistors. *IEEE Microw Magazine*. 2009;10(2):102-111. <https://doi.org/10.1109/mmm.2008.931675>.
  30. Reynoso-Hernández JA, Loo-Yau JR, Zuniga-Juarez JE, Valle-Padilla JLD. A straightforward method to determine the parasitic gate resistance of GaN FET. *IEEE MTT-S International Microwave Symposium Digest*, Boston, MA; 2009. <https://doi.org/10.1109/mwsym.2009.5165837>.
  31. Loo-Yau JR, Tapia-Sanchez I, Moreno P. An alternative method to extract the parasitic capacitances of GaN FETs. *Microw Opt Technol Lett*. 2015;57(1):223-225. <https://doi.org/10.1002/mop.28816>.
  32. Dambrine G, Cappy A, Heliodore F, Playez E. A new method for determining the FET small-signal equivalent circuit. *IEEE Trans Microw Theory Techn*. 1988;36(7):1151-1159. <https://doi.org/10.1109/22.3650>.
  33. Hughes B, Tasker PJ. Bias dependence of the MODFET intrinsic model elements values at microwave frequencies. *IEEE Trans Electron Dev*. 1989;36(10):2267-2273. <https://doi.org/10.1109/16.40909>.
  34. Berroth M, Bosch R. Broad-band determination of the FET small-signal equivalent circuit. *IEEE Trans Microw Theory Tech*. 1990;38(7):891-895. <https://doi.org/10.1109/22.55781>.
  35. Gonçalves CF, Nunes LC, Cabral PM, Pedro JC. Pulsed I/V and S-parameters measurement system for isodynamic characterization of power GaN HEMT transistors. *Int J RF Microw Comp-Aided Eng*. 2018;28:e21515. <https://doi.org/10.1002/mmce.21515>.
  36. Santarelli A, Cignani R, Gibiino GP, et al. A double-pulse technique for the dynamic I/V characterization of GaN FETs. *IEEE Microw Wirel Comp Lett*. 2014;24(2):132-134. <https://doi.org/10.1109/lmwc.2013.2290216>.
  37. Perez-Wences C, Loo-Yau JR and Moreno P. Simple and low-cost measurement test setup to determine the RF, LO and IF impedances for designing GaN FET resistive mixer. *IEEE 62nd International Midwest Symposium on Circuits and Systems (MWSCAS)*, Dallas, TX; 2019; 544-547. doi: <https://doi.org/10.1109/MWSCAS.2019.8884891>

## AUTHOR BIOGRAPHIES



**Daniel Ochoa Armas** was born in Havana, Cuba, in 1986. He received the BS in Electronics and Telecommunications Engineering and the MS in Telecommunications and Telematics degrees from the Technological Institute of Havana, Havana, Cuba, in 2009 and 2016, respectively. He is currently working toward a PhD degree in Electronic Design at the Centro de Investigación y Estudios Avanzados del I. P. N. Unidad Guadalajara (Cinvestav-GDL). His current research interests include nonlinear modeling

of semiconductors, and broadband and high-efficiency power amplifiers.



**Ismary Lavandera Hernández** was born in Havana, Cuba, in 1987. She received the BS in Electronics and Telecommunications Engineering and the MS in Telecommunications and Telematics degrees from the Technological Institute of Havana, Havana, Cuba, in 2010 and 2014, respectively. She is currently working toward a PhD degree in Electronic Design at the Centro de Investigación y Estudios Avanzados del I. P. N. Unidad Guadalajara (Cinvestav-GDL). Her current research interests include nonlinear modeling of semiconductors, and broadband and high-efficiency power amplifiers.



**Daniel Fernández** was born in Toluca, Mexico, in 1986. He received the Bachelor of Science in Electronics and Communications Engineering from the Universidad de Guanajuato, Guanajuato, Mexico, in 2014, and the M.Sc. degree in Electrical Engineering from the Centro de Investigación y Estudios Avanzados del I. P. N. Unidad Guadalajara, Guadalajara, Jalisco, México, in 2019. His research interests include Microwave Application like the characterization and the modeling of high-power devices (eg, GaN, etc.).



**José R. Loo-Yau** was born in Panamá, Panamá. He received the BSEE from the Universidad Autónoma de Guadalajara (U.A.G.) in 1998. In 2000, he received the MS in electronics and telecommunications from the Centro de Investigación Científica y de Educación Superior de Ensenada (CICESE.). From 2000 to 2002, he was a professor at the Faculty of Electronic Engineering at the UAG. In 2006, he received the DS in Electronics and Telecommunications with a specialty in high-frequency electronics from CICESE. He has worked as a design engineer for companies such as Zenith (Electro Partes de Matamoros) and PC Access. In 2007, he joined the electronic design group at the Centro de Investigación y Estudios Avanzados del I.P.N. Unidad Guadalajara as a researcher professor. In 2016, he was the interim president of the Microwave Theory and Techniques Guadalajara chapter and was a member of the organizing committee of the first IEEE Latin American Microwave Conference (IEEE LAMC). His research

interest is linear and nonlinear modeling of microwave transistors, power amplifiers, linearization of power amplifiers, and design of R.F. active circuits.



**Marlon Molina Ceseña** received the BSc degree in electronic engineering from the Autonomous University of Baja California, Ensenada, Baja California, Mexico, in 2014, the MSc degree in Electronics and Telecommunications with orientation in High-Frequency Electronic from the Center for Scientific Research and Higher Education of Ensenada (CICESE), Ensenada, Baja California, Mexico, in 2017, and is currently working toward the PhD degree at CICESE. He is currently with the RF and Microwave electronics group in the Applied Physics Division, CICESE. His research interests are small- and large-signal modeling and power transistors characterization using High- and Low-Frequency Load-Pull measurements.



**Caín Pérez-Wences** received the BS degree in Electronic Design Engineering from the Zapopan Superior Technological Institute, Guadalajara, Jalisco, México, in 2010, the MSc and DSc degrees in Electronic Design from the Centro de Investigación y Estudios Avanzados del I.P.N. Unidad Guadalajara (Cinvestav-GDL), Guadalajara, México, in 2015 and 2019, respectively. In 2020, he joined the Research and Technical Assistance Center of the State of Queretaro in Guadalajara (CIATEQ-GDL), Guadalajara, Jalisco, México, as an Electronics Lab Leader. His research interests include linear and nonlinear GaN and GaAs FET modeling, mixers, filters, high-efficiency power amplifiers, power-amplifier linearization techniques, and power-amplifier behavioral modeling.



**Ernesto A. Hernández-Domínguez** received the Electronic Design and Intelligent Systems Engineering degree from the Centro de Enseñanza Técnica Industrial (CETI), Guadalajara, Jalisco, México, in 2018, the MSc degree in Electric Engineering from the Centro de Investigación y Estudios Avanzados del I.P.N. Unidad Guadalajara (Cinvestav-GDL), Guadalajara, Jalisco, México, in 2020, and is currently working toward the PhD degree in Electric Engineering at the Cinvestav-Guadalajara.

His current research interests include active devices nonlinear modeling, frequency multipliers design and calibration techniques.



**J. Apolinario Reynoso-Hernández** was born in Tacupa Michoacán, Mexico. He received the Electronics and Telecommunications Engineering degree, from ESIME-IPN, Zatenco, Mexico, in 1984, MSc degree in Solid State Physics from CINVESTAV-IPN, Zatenco, Mexico in 1985 and DEA and PhD degree in Electronics, from Université Paul Sabatier-LAAS du CNRS, Toulouse, France in 1987 and 1989, respectively. In 1990, he joined Department of the Electronics and Telecommunications of CICESE in Ensenada, BC, Mexico where he is currently a Professor. His areas of specialized research interest include, high frequency on-wafer measurements, high frequency device modeling, linear and nonlinear active device characterization and modeling. He has leaded CICESE's Microwave group to obtain the best interactive forum paper award five times. Since 2013, he has served as TPC of ARFTG and ARFTG-MTT Work shop organizer 2019 and 2020. He has been a Reviewer for many IEEE journals



**Pablo Moreno**, received the Electrical and Mechanical Engineering degree from the Universidad Nacional Autónoma de México (UNAM), Mexico, in 1985, the M.S.E.E. degree from the Instituto Tecnológico y de Estudios Superiores de Monterrey (ITESM), Mexico, in 1989, and the PhD degree in electrical engineering from Washington State University, Washington, in 1997. In 1998, he joined the Faculty of the Center for Research and Advanced Studies of Mexico (CINVESTAV) Campus Guadalajara, Guadalajara, Mexico. His research interests include applied electromagnetics and low and high frequency transmission lines modeling.

**How to cite this article:** Ochoa-Armas D, Lavandera-Hernández I, Fernández-Ramón D, et al. A nonlinear empirical I/V model for GaAs and GaN FETs suitable to design power amplifiers. *Int J RF Microw Comput Aided Eng.* 2021;31: e22552. <https://doi.org/10.1002/mmce.22552>